

# Performance tests of an AGIPD 0.4 assembly at the beamline P10 of PETRA III

---

**J. Becker<sup>a\*</sup>, A. Marras<sup>a</sup>, A. Klyuev<sup>a</sup>, F. Westermeier<sup>a</sup>, U. Trunk<sup>a</sup>, and H. Graafsma<sup>a,b</sup>**

<sup>a</sup>*Deutsches Elektronen-Synchrotron (DESY),  
Notkestr. 85, 22607 Hamburg, Germany*

<sup>b</sup>*Mid Sweden University,  
Holmgatan 10, S-85170 Sundsvall, Sweden*

**ABSTRACT:** The Adaptive Gain Integrating Pixel Detector (AGIPD) is a novel detector system, currently under development by a collaboration of DESY, the Paul Scherrer Institute in Switzerland, the University of Hamburg and the University of Bonn, and is primarily designed for use at the European XFEL. To verify key features of this detector, an AGIPD 0.4 test chip assembly was tested at the P10 beamline of the PETRA III synchrotron at DESY. The test chip successfully imaged both the direct synchrotron beam and single 7.05 keV photons at the same time, demonstrating the large dynamic range required for XFEL experiments. X-ray scattering measurements from a test sample agree with standard measurements and show the chip's capability of observing dynamics at the microsecond time scale.

**KEYWORDS:** AGIPD; PETRA III; adaptive gain; burst mode imaging.

---

\*Corresponding author. E-mail: Julian.Becker@desy.de

---

## Contents

<b>1. Introduction</b>	<b>1</b>
<b>2. The AGIPD 0.4 assembly</b>	<b>2</b>
2.1 Operation parameters and data acquisition	2
2.1.1 Patterns	3
2.1.2 Experimental limitations	3
<b>3. The P10 beamline</b>	<b>4</b>
<b>4. Results</b>	<b>5</b>
4.1 Measurements without sample	5
4.2 Measurements with sample	7
4.3 Burst mode	8
4.3.1 Intensity autocorrelation	9
<b>5. Summary</b>	<b>10</b>

---

## 1 Introduction

The Adaptive Gain Integrating Pixel Detector (AGIPD) is a novel detector system currently under development by a collaboration of DESY, the Paul Scherrer Institute in Switzerland, the University of Hamburg and the University of Bonn [1, 2]. It was designed for use at the European XFEL [3, 4] and will be able to cope with the demanding requirements of this machine for 2D imaging systems. The European XFEL will provide pulse trains, consisting of up to 2700 pulses separated by 220 ns (600  $\mu$ s in total) followed by an idle time of 99.4 ms, resulting in a supercycle of 10 Hz and 27000 pulses per second. The energy of the X-rays will be tunable, and the tuning range will depend on the experimental station.

AGIPD is based on the hybrid pixel technology and aimed at imaging in the energy range between 3 and 15 keV. The current design goals of the newly developed Application Specific Integrated Circuit (ASIC) with independent dynamic gain switching amplifier in each pixel are a dynamic range of more than  $10^4$  12.4 keV photons (for each pixel) in the lowest gain, single photon sensitivity in the highest gain, and operation at 4.5 MHz frame rate.

Due to the special pulse structure of the European XFEL, it is necessary to store the acquired images inside the pixel circuit area during the pulse train. A compromise had to be found between storing many images, requiring a large pixel area, and high spatial resolution, requiring small pixel sizes [1, 2]. The AGIPD will feature a pixel size of  $(200 \mu\text{m})^2$ , which is sufficient to accommodate an analog memory for 352 images. An external veto signal can be provided to maximize the number

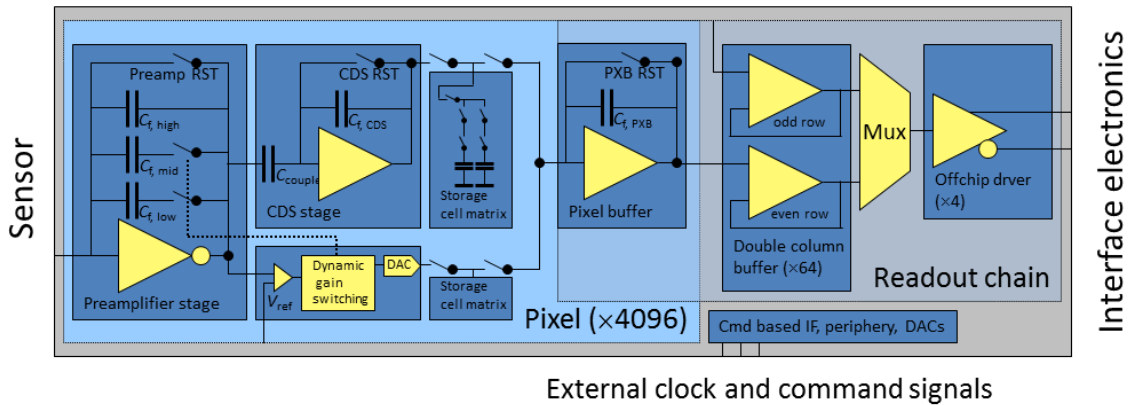


Figure 1. Circuit diagram of AGIPD 1.0.

20 of useful images by overwriting any image previously recorded during the pulse train. The image  
 21 data is read out and digitized in the 99.4 ms between pulse trains.

22 Testing and calibration of novel detector systems is of essential importance for their perfor-  
 23 mance. As it is very hard to approximate the properties of free electron laser sources using com-  
 24 monly available lab sources, beam tests at synchrotron sources are helpful to verify important  
 25 functional parameters of the detector system. In the following we will present the results of a  
 26 performance tests of AGIPD 0.4 at the synchrotron beamline P10 at PETRA III.

## 27 2. The AGIPD 0.4 assembly

28 The AGIPD 0.4 assembly is a 16x16 pixel prototype of the AGIPD, bump bonded to a silicon  
 29 sensor. The pixels have the same size as the final system,  $(200 \mu\text{m})^2$ , and feature the adaptive gain  
 30 switching amplifier with 3 stages and 352 storage cells per pixel. A block diagram of the full scale  
 31 chip is shown in Figure 1. The detector assembly was mounted on a daughter card on the movable  
 32 detector table and connected to a custom made chip tester box with cables<sup>1</sup>. The chip tester box  
 33 handled all communication with the ASIC. In contrast to the sensor thickness intended for the full  
 34 scale detector (500  $\mu\text{m}$ ), the ASIC was bump bonded to a silicon sensor of 320  $\mu\text{m}$  thickness having  
 35 a depletion voltage of approximately 50 V. To (over-)deplete the sensor, a bias voltage of 120 V  
 36 was applied. All measurements were performed without cooling at room temperature.

### 37 2.1 Operation parameters and data acquisition

38 As the chip tester box was designed for testing, communication and data acquisition is based on  
 39 patterns (explained below) rather than images. Communication with the chip tester box occurs over  
 40 a TCP/IP network.

41 The chip tester box communicates with the test chip by providing input signals (called vectors)  
 42 on all input lines and digitizing the output of the analog output of the ASIC. All commands to the  
 43 ASIC are constructed by sending a sequence of vectors.

<sup>1</sup>In this respect the setup is different from the usual lab setup. The additional noise introduced by the cables is minimal.

44 Some commands (e.g. the selection of a memory cell) require a fixed number of clock cycles  
45 to perform. Other commands, e.g. the reset of the preamplifier, require a defined time to perform  
46 and the number of required clock cycles depends on the master clock frequency.

### 47 **2.1.1 Patterns**

48 The vectors to be sent to the ASIC are generated inside the Field Programmable Gate Array (FPGA)  
49 of the chip tester box. This FPGA is programmed to send a pattern (a stream of vectors) to the  
50 ASIC. Due to the limited amount of memory inside the FPGA the maximum number of vectors  
51 in a pattern is limited. During the sending of the pattern the Analog-to-Digital Converter (ADC)  
52 on the chip tester board continuously samples the output of the ASIC into a FIFO (First In, First  
53 Out) buffer. Upon completion of the pattern the digitized output data is sent to the controlling PC  
54 over the network connection. A new acquisition cycle cannot start before the last data packet has  
55 successfully arrived at the PC.

56 Since the amount of commands sent to the ASIC in sequence is limited, the chosen master  
57 clock frequency of 5 MHz is a compromise between a high value, allowing high frame rates, and  
58 the number of commands that can be stored into the memory of the FPGA. It allowed to compose  
59 the following two patterns that were used for the experiments:

- 60 • Imaging pattern: This pattern was used for the experiments in imaging mode. It integrates  
61 for 200 ns (1 clock cycle) in all pixels before reading the analog and gain information of all  
62 16x16 pixels in a defined sequence.
- 63 • XPCS pattern: This pattern was used for the X-ray Photon Correlation Spectroscopy (XPCS)  
64 experiments. It integrates for 200 ns, then reads the analog information of a single pixel. This  
65 process is repeated 314 times, and the time between the beginning of two integration periods  
66 is 9.6  $\mu$ s.

67 The chip can image at 4.5 MHz and more, but as XPCS experiments critically depend on the  
68 number of frames recorded in sequence it was decided to run at lower speed and capture more  
69 frames in a single pattern<sup>2</sup>.

### 70 **2.1.2 Experimental limitations**

71 At the time of the test no bunch clock was available at P10. This led to the effects explained in the  
72 following paragraph.

73 In operation the preamplifier is sensitive to charges collected in the sensor material during  
74 the integration phase as well as during the Correlated Double Sampling (CDS) reset phase, which  
75 happens immediately before the integration phase. All charge (and equivalent noise charge, esp.  
76 the noise from the release of the preamp reset switch) that is accumulated during the CDS reset  
77 phase is removed by the CDS mechanism. This mechanism is ideally suited to reduce the effective  
78 noise of the system when properly synchronized to a pulsed source in such a way that no signal  
79 charge is accumulated during the CDS reset phase<sup>3</sup>.

---

<sup>2</sup>The length of the sequence is defined by the number of frames recorded in a single pattern.

<sup>3</sup>When the operating conditions of the preamplifier change (i.e. by switching gain) during the integration time the double sampling is no longer correlated and its benefit is reduced. It should be noted that this has no impact on the detector performance as larger noise can be tolerated at the large signals required to trigger the gain switching.

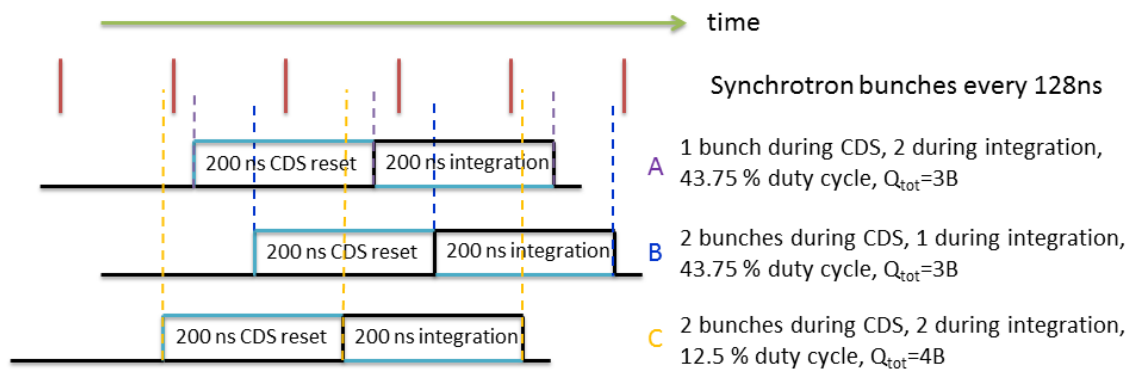


**Figure 2.** The three different possibilities to distribute bunches every 128 ns during the CDS reset and integration phase.

80 During the experiment three possible situations, depicted in Figure 2, were possible: A) 1  
 81 bunch arrives during the CDS reset phase, 2 bunches during the integration phase, B) 2 bunches  
 82 arrive during the CDS reset phase, 1 bunch during the integration phase or C) 2 bunches arrive both  
 83 during CDS reset and integration phase.

84 Knowing that CDS reset and integration phase are each 200 ns long and that bunches come  
 85 every 128 ns, one can calculate the duty cycles of case A) and B) to be 43.75% each and case  
 86 C) to be 12.5%. If one bunch deposits, on average, a charge of  $1B$ , than cases A) and B) have  
 87 the preamplifier swing from 0 to  $1B$  or  $2B$  after the CDS reset phase and to  $3B$  after the integration  
 88 phase, while case C) swings the preamplifier from 0 to  $2B$  to  $4B$ . The output of the chip is  $3B - 1B =$   
 89  $2B$  for case A),  $3B - 2B = 1B$  for case B) and  $4B - 2B = 2B$  for case C). It should be noted that  
 90 the preamplifier in case C) operates at a different working point than in case A) which may lead to  
 91 different ASIC outputs of cases A) and C), especially if the preamplifier leaves its linear regime for  
 92 charges greater than  $3B$ .

### 93 3. The P10 beamline

94 The coherence beamline P10 at PETRA III operates in the medium-hard x-ray regime (5-25 keV).  
 95 For the AGIPD 0.4 chip test described here the photon energy was set to 7.05 keV and PETRA III  
 96 was running in 60 bunch mode, resulting in a photon pulse approximately every 128 ns. The total  
 97 flux at the sample position was estimated using a calibrated diode and a reference scatterer to be  
 98  $1-2 \times 10^{11}$  photons/s.

99 The monochromatized beam was focused at sample location to a size of approximately  $5 \mu\text{m}$   
 100  $\times 3 \mu\text{m}$ , which corresponds to a size of approximately  $350 \mu\text{m} \times 175 \mu\text{m}$  (vert.  $\times$  horiz.) in the  
 101 detector plane. A sketch of the experimental setup is shown in Figure 3. The distance between the  
 102 sample and the detector plane was 5.2 m.

103 The sample consisted of silica particles with a nominal radius of 250 nm suspended in water.  
 104 The particle concentration was chosen such that the sample can be considered dilute (spheres are  
 105 diffusing freely) and any effects of interparticle interactions can be neglected.

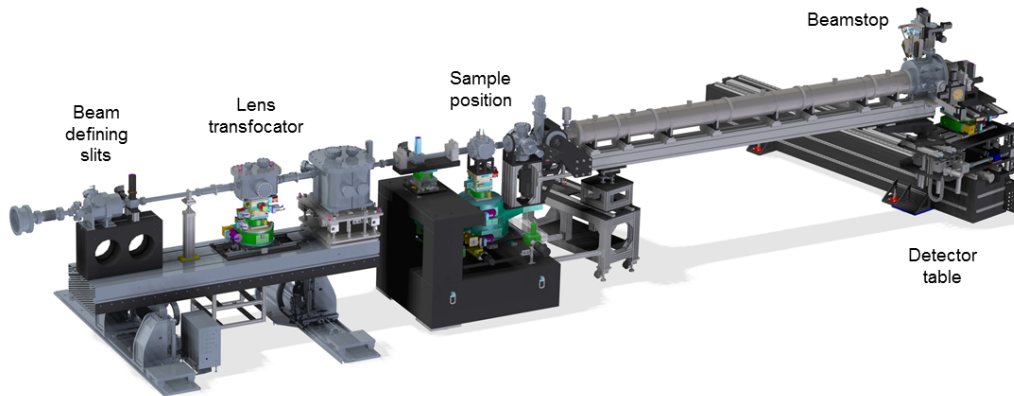


**Figure 3.** Experimental setup at the P10 beamline. Upstream of the sketched setup the X-ray beam passes several optics elements including a monochromator and enters the sketched setup from the left side.

## 106 4. Results

107 Except for the region very close to the primary beam, the images are virtually empty as the inte-  
 108 gration time of 200 ns is very short. Simply summing up frames would overemphasize the noise of  
 109 the system, therefore the data was analyzed in a post-processing counting mode [5].

110 In this counting mode every individual frame was analyzed separately. A global noise cut  
 111 threshold was applied and the energy above threshold detected by each pixel was quantized to a  
 112 discrete number of photons. This procedure is very similar to the signal processing inside the ASIC  
 113 of photon counting detectors like the Pilatus [6] or the Medipix [7], with two notable exceptions:  
 114 Multiple photon counts are registered correctly, and the threshold can be (re-)adjusted after the  
 115 data is acquired. A detailed study of the impact of different threshold settings including the charge  
 116 sharing effect has been presented in [8].

### 117 4.1 Measurements without sample

118 In order to test the dynamic range, images of the direct beam were recorded. An image averaged  
 119 from 3000 individual frames is displayed in Figure 4. The averaged image spans a dynamic range  
 120 of more than 6 orders of magnitude. This is not obvious from individual frames, as the pixels far  
 121 from the direct beam register no photons most of the time.

122 The X-ray beam was focused on the sample position, therefore it is defocused in the detector  
 123 plane. The known slight asymmetry<sup>4</sup> of the primary beam is observed, as the beam is wider in  
 124 vertical than in horizontal direction.

125 When looking at the histogram of the analog output of the pixel located one pixel to the left and  
 126 up from the central pixel (shown in Figure 5), the pulsed nature of PETRA III can be seen clearly.  
 127 The pixel is in medium gain mode and shows the behavior explained previously. Two distinct  
 128 peaks are easily observed and indicate that either one or two bunches are impinging on the detector  
 129 during the integration time. The peaks contain about 44% of the total number of counts each and

<sup>4</sup>Due to the different beam size and divergence in the horizontal and vertical plane.

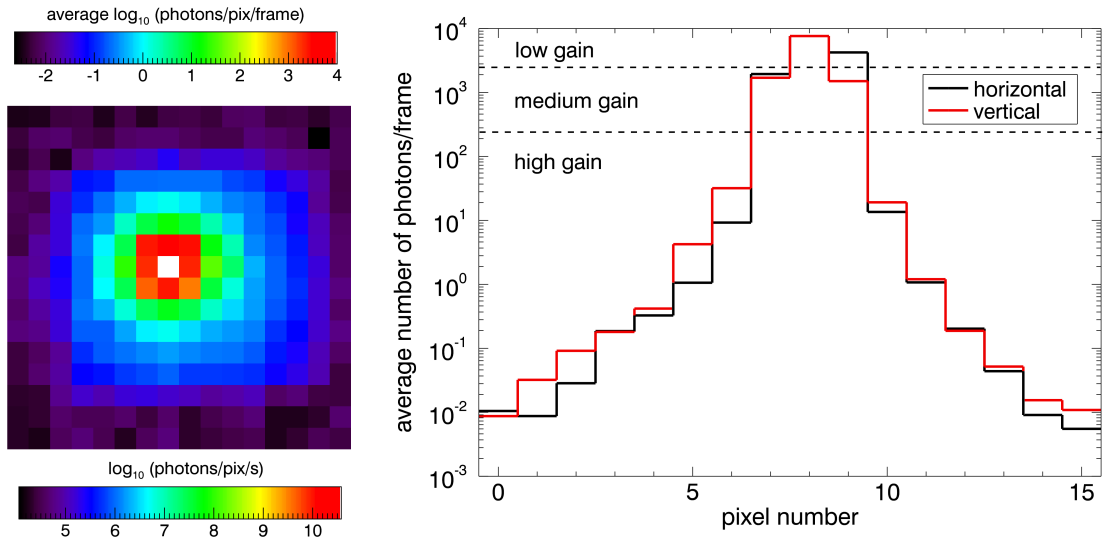


**Figure 4.** Left: Image of the direct beam. The color encodes the logarithm to the base 10 of the number of photons per pixel. Right: Line-cut of the left image along the horizontal and vertical direction through the most intense pixel. As indicated by the dashed lines, the image contains pixels in all three gain stages simultaneously.

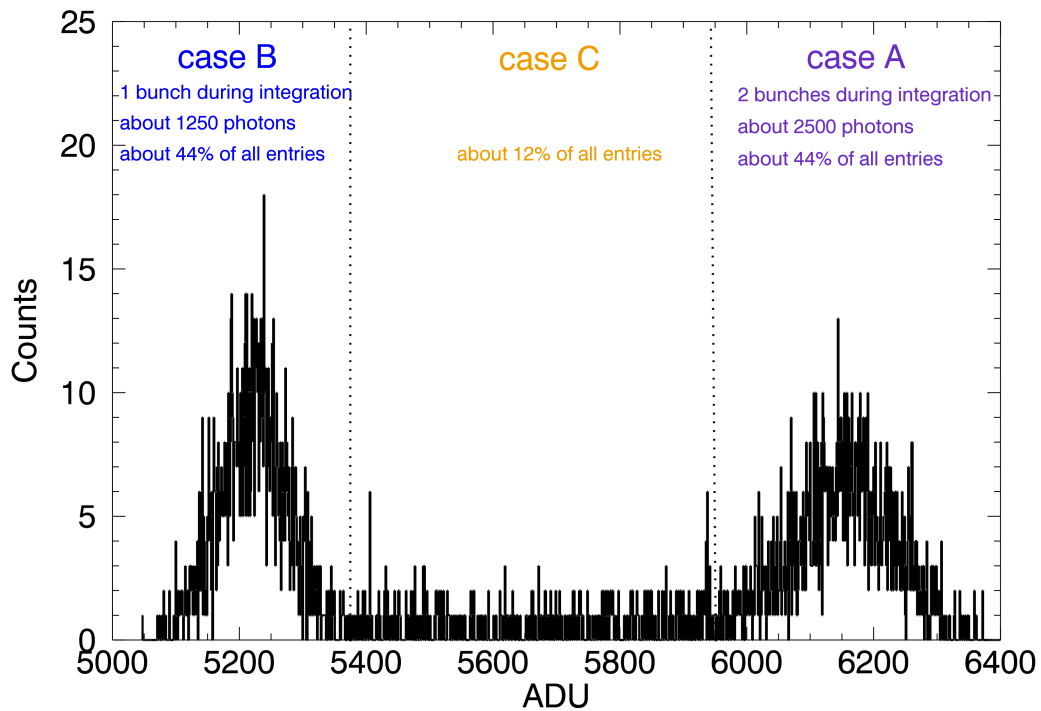


**Figure 5.** Histogram of the analog output of the pixel up and left of the most intense pixel. The pixel is in medium gain mode. The two peaks indicate that either one or two bunches are impinging on the detector during the integration time. Having no photons in second gain would correspond to around 4300 ADU; note that when no photons are present the detector is in high gain mode, so this value is an extrapolation.

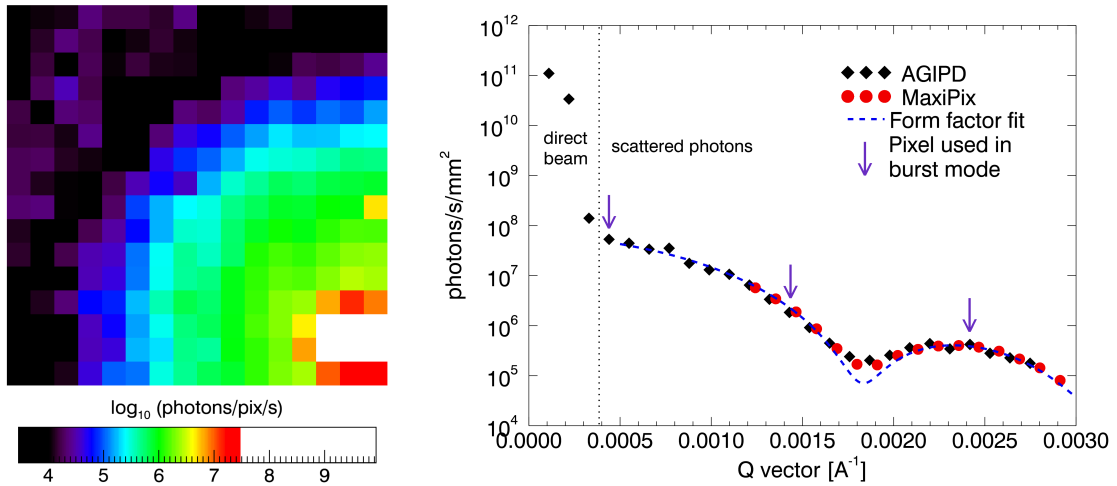


**Figure 6.** Left: Image of the scattering pattern of the sample. The color encodes the logarithm to the base 10 of the number of photons/s/pixel and has been restricted to the range from 4.0 to 7.5 to enhance the visibility of the ring structure. Right: Azimuthal average of the left image and comparison to data obtained with a MaxiPix detector. The dotted line indicates a particle form factor fit to the MaxiPix data.

130 the remaining 12% of counts are distributed in between them. These percentages correspond to the  
 131 duty cycle of the three different possibilities to distribute the bunches during the time the ASIC is  
 132 sensitive to charge collection in the sensor, as depicted in Figure 2.

133 Imaging the direct beam is a test for the dynamic gain switching; in each individual image  
 134 there are pixels in every gain stage. The central pixel is a special case, as it is operating outside of  
 135 the linear regime. It is not completely saturated, as the distinct two peak nature of the histogram is  
 136 still observable (not shown) and some corrections for the saturation behavior can be made.

137 Using the image displayed in Figure 4 the total flux of the beam can be calculated to be  
 138 approximately  $0.5 \times 10^{11}$  photons/s. This is lower by a factor of approximately 3 than the estimate  
 139 for the beam from the diode measurements, the reason for which is the partial saturation of the  
 140 central pixel.

## 141 4.2 Measurements with sample

142 Studying colloidal particles, a common sample system for small angle X-ray scattering and XPCS  
 143 experiments, is an efficient way of demonstrating the performance of the AGIPD 0.4 test chip.  
 144 These particles can be synthesized from different materials in a large variety of sizes and shapes.  
 145 Thereby their well known dynamics can be tailored to the specific task at hand [10]. In this exper-  
 146 iment we will look at the particle form factor of the sample and at equilibrium fluctuations in the  
 147 microsecond regime.

148 For the measurements a sample consisting of spherical colloidal particles with a nominal radius  
 149 of 250 nm was inserted at the focus position of the beam.

150 The image displayed in Figure 6 is an average of 10000 individual images and covers a dy-  
 151 namic range of more than 6 orders of magnitude. The color map of the image has been restricted  
 152 to 3.5 orders of magnitude to enhance the visibility of the diffraction pattern with a local maximum  
 153 at approximately  $0.0022 \text{ \AA}^{-1}$ . In addition, the same sample was imaged using a MaxiPix refer-

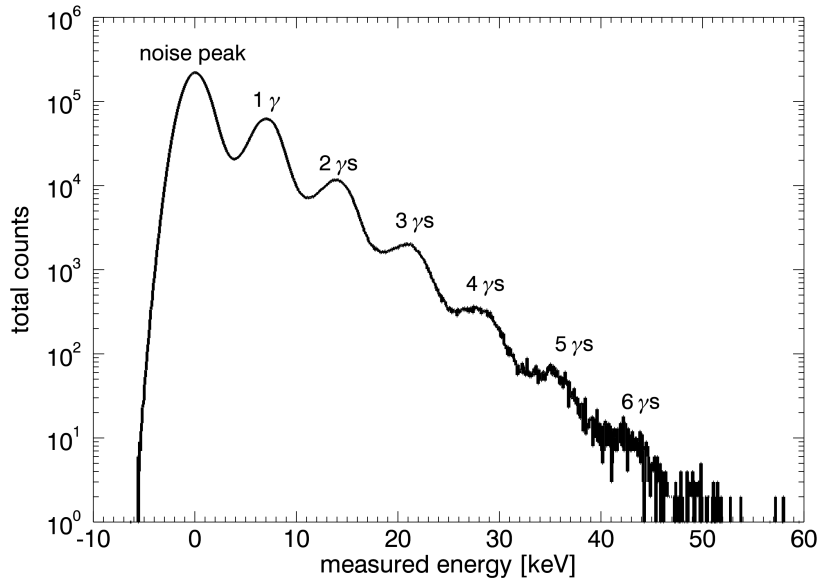


**Figure 7.** Histogram of the largest data set taken with the XPCS pattern. The average intensity is 0.3 photons per 200 ns, corresponding to a count rate of 1.5 Mcps/pixel or 37.5 Mcps/mm<sup>2</sup>. The individual peaks of photons of 7.05 keV are clearly distinguishable. The rms noise of this pixel is 320 electrons.

154 ence detector and the azimuthal average of the intensity distribution recorded with both detectors  
 155 is shown in the right hand side graph of Figure 6.

156 The dotted line is a fit of a spherical form factor (PQ-Fit) to the MaxiPix data. Only the  
 157 MaxiPix data was used for this fit, as the recorded data extends to large scattering vectors due to  
 158 the bigger detector area. The fit result for the particle radius is 245 nm.

159 It should be noted that no cross calibration between the two detector systems was performed.  
 160 The AGIPD data reproduces the extrapolation of the PQ-Fit towards lower scattering angles and  
 161 agrees with the intensity measured by the MaxiPix detector within the statistical errors.

162 In contrast to the MaxiPix detector, AGIPD 0.4 provides experimental data including the direct  
 163 beam (three leftmost data points). Usually the beamline is operated with a beamstop to protect the  
 164 detector from the direct beam, which blocks all signals below a certain scattering angle (approx-  
 165 imately 0.001 Å<sup>-1</sup> in this case).

### 166 4.3 Burst mode

167 Three pixels, at 0.00044 Å<sup>-1</sup>, 0.0014 Å<sup>-1</sup> and 0.0024 Å<sup>-1</sup>, were selected to perform XPCS exper-  
 168 iments using the dedicated XPCS pattern.

169 Figure 7 shows the counting statistics for the pixel at 0.00044 Å<sup>-1</sup>. Charge integration during  
 170 the CDS reset phase is negligible, as the average count rate of 0.3 photons/frame<sup>5</sup> uses only a very  
 171 tiny fraction of the dynamic range of the first gain stage (extending to about 1.1 MeV deposited  
 172 energy).

<sup>5</sup>Due to the short integration time of 200 ns this corresponds to 1.5 Mcps/pixel, or 37.5 Mcps/mm<sup>2</sup>.

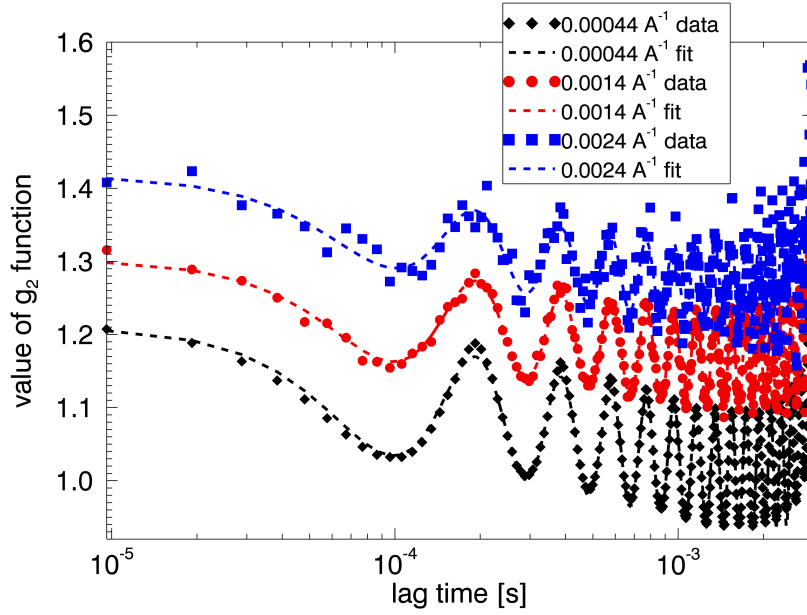


**Figure 8.**  $g_2$  functions derived from the XPCS data. The different scattering angles are indicated by the color. Symbols indicate the data points from the measurement, lines analytic fits to the data. The  $g_2$  functions have been horizontally offset for better visibility. AGIPD 0.4 allows determination of correlations on the microsecond timescale.

173 The investigated pixel has a noise of approximately 320 electrons rms, which is consistent  
 174 with previous noise measurements [11]. This pixel fulfills the criteria for single photon detection at  
 175 the European XFEL [8]. Figure 7 shows a clear separation up to 6 photons, at which point statistics  
 176 limit the unanimous identification of further peaks.

#### 177 4.3.1 Intensity autocorrelation

178 The intensity autocorrelation function ( $g_2$  function) is both a measure of the correlation time and  
 179 the speckle contrast of a system. Details on this analysis type can be found in textbooks like [12],  
 180 specific details for XPCS using the AGIPD can be found here [13, 14].

181 With our setup the bunch frequency of PETRA III cannot be measured directly; however, the  
 182 pulsed nature is still observable with a lower apparent frequency that is determined by the aliasing  
 183 effect.

184 The apparent frequency  $f_{alias}$  expected from the aliasing effect can be calculated from the true  
 185 frequency  $f_{true}$ , the sampling frequency  $f_{sampling}$  and an integer number  $N$ :

$$f_{alias} = |f_{true} - Nf_{sampling}|. \quad (4.1)$$

186 Using the orbital length<sup>6</sup> of the storage ring  $L_{PETRA}$ , the speed of light  $c$ ,  $M = 60$  the number  
 187 of bunches, the sampling frequency  $f_{sampling} = 1/9.602\mu s = 104.145kHz$  and  $N = 75$  we obtain  
 188 the following frequency expected for our experiments:

<sup>6</sup>This is the 2.3 km circumference of PETRA III. A high precision value of this dimension (accurate to 1 cm) was calculated from the radio frequency of the machine.

$$f_{alias} = \left| \frac{cM}{L_{Petra}} - Nf_{sampling} \right| = 5.185 \text{ kHz}. \quad (4.2)$$

189 Figure 8 shows the  $g_2$  functions derived from the data (symbols) accompanied by lines repre-  
 190 senting the analytic fit to the data points.

191 It is readily observable that the  $g_2$  functions do not follow the expected monotonic decrease,  
 192 but show a characteristic oscillation with a local minimum at a lag time of approximately  $10^{-4}$  s.  
 193 The analytic fits identify the oscillation frequency to be 5.18 kHz, which is the expected aliased  
 194 bunch repetition frequency.

195 Additionally, all functions show a 'hockey stick' behavior for lag times above approximately  
 196  $10^{-4}$  s. They decrease more than expected from the sample dynamics<sup>7</sup>, show a local minimum  
 197 (overlaid by the oscillations) between 1 and  $2 \times 10^{-3}$  s and increase to an off-scale value for the  
 198 last few data points. This behavior is caused by the limited number of frames.

199 Emphasis should be put on the timescale of the study, not on the studied physics. The relevant  
 200 timescales that are within reach of the correlation analysis are on the order of several microseconds.  
 201 In addition it should be noted that for this type of analysis the reliable detection of individual  
 202 photons is mandatory and achieved by AGIPD 0.4.

## 203 5. Summary

204 An AGIPD 0.4 test chip was installed at the P10 beamline and several prototypical experiments  
 205 were performed. Although it is a prototype, all components relevant for operation at the European  
 206 XFEL are present.

207 The direct beam was imaged successfully, thereby demonstrating that the large dynamic range  
 208 required for XFEL applications (single photons and  $10^4$  12 keV photons simultaneously in a single  
 209 frame) is achieved.

210 The single photon sensitivity required for experiments at the European XFEL (ENC of less  
 211 than 340 electrons) was shown and individual 7 keV photons could be distinguished. Please note  
 212 that in the original design of the detector operation at a fixed beam energy of 12.4 keV was antici-  
 213 pated.

214 The intensity fluctuation analysis of the colloidal sample demonstrated the burst mode ca-  
 215 pability, which is essential for usage at the European XFEL. Correlations at the level of several  
 216 microseconds were observed, which makes AGIPD 0.4 one of the fastest 2D imaging detectors  
 217 currently available.

## 218 Acknowledgments

219 The authors would like to thank DESY and especially the PETRA III facility for access to the  
 220 beamline, the European XFEL for co-funding the development of AGIPD, the entire team that  
 221 designed, produced and assembled AGIPD 0.4 and Bernd Struth and Michael Sprung for their  
 222 input.

---

<sup>7</sup>This is only visible when compared to detailed simulations, which are beyond the scope of this paper.

223 **References**

- 224 [1] B. Henrich et. al., *The adaptive gain integrating pixel detector AGIPD a detector for the European*  
225 *XFEL*, Nucl. Instr. and Meth. A 633(1) 2011 S11-14, DOI: 10.1016/j.nima.2010.06.107.
- 226 [2] X. Shi et. al., *Challenges in chip design for the AGIPD detector*, Nucl. Instr. and Meth. A 624(2)  
227 2010 387-391, DOI: 10.1016/j.nima.2010.05.038.
- 228 [3] M. Altarelli et al., *European X-ray free electron laser: Technical design report*, ISBN  
229 978-3-935702-17-1 (2006).
- 230 [4] T. Tschentscher et al., *Layout of the X-Ray Systems at the European XFEL*, Technical Note XFEL.EU  
231 TN-2011-001 (2011) DOI: 10.3204/XFEL.EU/TR-2011-001.
- 232 [5] H. T. Philipp et al., *Low-flux measurements with Cornell's LCLS integrating pixel array detector*, J.  
233 *Inst.* 6 2011, doi:10.1088/1748-0221/6/11/C11006.
- 234 [6] B. Henrich et.al., *PILATUS: A single photon counting pixel detector for X-ray applications*, Nucl.  
235 *Instr. and Meth. A* 607(1) 2009, 247-249, DOI: 10.1016/j.nima.2009.03.200.
- 236 [7] R. Ballabriga et al., *The Medipix3 prototype, a pixel readout chip working in single photon counting*  
237 *mode with improved spectrometric performance*, *Nuclear Science, IEEE Transactions on*, vol. **54**, pp.  
238 1824 –1829, oct. 2007.
- 239 [8] J. Becker et al., *The single photon sensitivity of the Adaptive Gain Integrating Pixel Detector*, Nucl.  
240 *Instr. and Meth. A* 694(1) 2012 82-90, doi:10.1016/j.nima.2012.08.008.
- 241 [9] F. Westermeier, *Structure and Dynamics of highly charged colloidal suspensions*, PhD Thesis  
242 Hamburg university 2010.
- 243 [10] F. Westermeier et al., *Structure and short-time dynamics in concentrated suspensions of charged*  
244 *colloids*, *J. Chem. Phys* 137(11) 2012 114504, DOI: 10.1063/1.4751544.
- 245 [11] D. Greiffenberg et al., *Optimization of the noise performance of the AGIPD prototype chips*,  
246 submitted to *J. Instr.*
- 247 [12] G. Grübel, A. Madsen, and A. Robert in *Soft-Matter Characterization*, Ch. 18, p. 953-995, R. Borsali  
248 & R. Pecora (Eds.), (Springer, 2008).
- 249 [13] J. Becker, C. Gutt, H. Graafsma, *Simulation study of the impact of AGIPD design choices on X-ray*  
250 *Photon Correlation Spectroscopy utilizing the intensity autocorrelation technique*, *J. Inst.* **6** 2011  
251 P11005.
- 252 [14] J. Becker and H. Graafsma, *Advantages of a logarithmic sampling scheme for XPCS experiments at*  
253 *the European XFEL using the AGIPD detector*, *J. Inst.* **7** 2012 P04012.